JOURNAL OF SPACECRAFT AND ROCKETS
Vol. 30, No. 6, November–December 1993

Fin-Planform Effects on Lift and Center of Pressure for Supersonic Missiles

H. F. Nelson* and M. V. Talpallikar†
University of Missouri-Rolla, Rolla, Missouri 65401

The missile fin-body interference factor $K_{W(B)}$ (ratio of the normal force on a fin in presence of the missile body to the normal force on the isolated fin) is an important factor in the equivalent angle-of-attack preliminary design method. A finite volume Euler code, ZEUS, is used to numerically determine the fin forces as a function of fin trailing-edge sweep for 2-, 3-, 4-, 5-, and 6-fin missile configurations at small angles of attack. The fin forces are used to evaluate $K_{W(B)}$ as a function of fin span to body radius ratio at Mach numbers from 2.5 to 5 at various fin aspect ratios. The movement of center of pressure with changes in trailing-edge sweep and Mach number is also evaluated. $K_{W(B)}$ and center of pressure values for the 2-, 3-, and 4-fin configurations agree with slender-body theory analytical solutions; however, the $K_{W(B)}$ predictions for the 5- and 6-fin missiles break away from slender-body theory as the fin span increases. The fin span at which breakaway occurs is shown to be related to the position at which shock and expansion waves originating from the adjacent fins strike the fin of interest; consequently, it is a function of number of fins and Mach number. In some cases the shock and expansion wave interaction cause $K_{W(B)}$ to be <1, which indicates a reduction in fin lift due to interference. Tables for $K_{W(B)}$ and the center of pressure are presented for use in preliminary design.

Nomenclature

AR	= aspect ratio of wing formed by joining two fins
A_W	= area of wing formed by two fins joined at root chord
CP	= center of pressure
$K_{W(B)}$	= fin-body interference factor due to upwash
K_ϕ	= fin-fin interference factor due to sideslip
L_W	= lift of wing alone
$L_{W(B)}$	= lift of the wing in the presence of body
M_∞	= freestream Mach number
P	= pressure
q_∞	= freestream dynamic pressure
R	= missile fuselage radius
S	= fin span, measured from body centerline
S/R	= ratio of fin span to body radius
x, y, z	= axes; origin at missile nose
y_{CP}	= fin radial CP position (see Fig. 1)
y_{ND}	$= y_{CP}/R$
z_{LE}	= fin root-chord leading-edge axial position
z_{CP}	= fin axial CP position (see Fig. 1)
z_{ND}	= nondimensional fin CP axial position = $(z_{CP} - z_{LE})/R$
z/R	= ratio of z location to fuselage radius
α	= missile angle of attack
α_{eq}	= equivalent angle of attack
α_F	= fin angle of attack
β	= missile sideslip angle
β_F	= fin sideslip angle
$(\Delta\alpha_{eq})_V$	= induced change in α due to vortices
ϵ	= fin leading-edge semivertex angle
τ	= fin trailing-edge semivertex angle

Received July 16, 1990; revision received June 8, 1992; accepted for publication Dec. 8, 1992.

*Professor of Aerospace Engineering, Thermal Radiative Transfer Group, Department of Mechanical and Aerospace Engineering and Engineering Mechanics. Associate Fellow AIAA.

†Graduate Student, Department of Mechanical and Aerospace Engineering and Engineering Mechanics; currently CFD Research Corporation, Huntsville, AL 35805. Member AIAA.

Introduction

PRELIMINARY design and performance estimation of missile configurations requires rapid, accurate methods to predict the effects of 1) aerodynamic coupling between the missile body and the fins and 2) shock and expansion wave interactions between adjacent fins on the fin forces and moments. These methods are especially important for tradeoff studies in preliminary and conceptual design. Two different numerical approaches can be employed to calculate missile aerodynamic characteristics: computational fluid dynamics or approximate codes using empirical and analytical methods. Computational fluid dynamics solves the complete set of flowfield equations for general freestream conditions and body shapes. These solutions, typically obtained using the Euler or Navier-Stokes equations, are more accurate than the empirical methods; however, they are difficult to obtain and are computer intensive. These difficulties preclude their general use in preliminary design where rapid design tools are needed.

The empirical approach employs approximate linear and nonlinear analyses as well as experimental data. Considerable research is still needed to improve and extend these prediction tools, especially in the areas of improved accuracy, extended scope of applicability, ease of use, and robustness. Two distinct techniques comprise the bulk of this approach; namely, component buildup methods and paneling methods.[1]

Currently, many preliminary design correlations are based on component buildup methods. These methods predict the aerodynamic characteristics of the total airframe by summing up the aerodynamic characteristics of the major airframe components in isolation (e.g., body, wing, tail, etc.) and then adding to those sums the loads produced by component interference. For tactical missile designs the interference effects are often first order and nonlinear. The key to component buildup methods is to adequately estimate the interference effects. Slender-body theory has been used in the past.[2] In the current research the Euler equations are used.

Equivalent Angle of Attack

Component buildup techniques are most easily applied using the equivalent angle-of-attack method.[3-8] This method predicts the nonlinear lifting characteristics of missile fins in terms of the equivalent angle of attack and it incorporates complicated aerodynamic nonlinearities in terms of interfer-

ence factors. The interference factors are multiplied by the fin-alone forces to give the force on the fin in the presence of the body. The equivalent angle of attack is defined as

$$\alpha_{eq} = K_{W(B)}\alpha_F + 4K_\phi\alpha_F\beta_F/AR + (\Delta\alpha_{eq})_V \quad (1)$$

in terms of interference factors K_ϕ and $K_{W(B)}$. There are three separate contributions to the calculation of the missile normal-force coefficient: 1) the fin-body carryover interference factor $K_{W(B)}$; 2) the influence of combined angle of attack and sideslip angle K_ϕ; and 3) the influence of external vortices $(\Delta\alpha_{eq})_V$. The equivalent angle-of-attack method is derived and its accuracy is demonstrated in Ref. 3. Extensions of the method to high angles of attack are discussed in Refs. 4 and 5.

$K_{W(B)}$ is the ratio of lift produced by a fin in presence of the body to the lift produced by the fin alone.[9] K_ϕ is the ratio of the change in the normal force on a fin, in the presence of the body and other fins, caused by the change in sideslip angle to the normal force on the fin alone. The third term represents the effect of vortex interactions. It can be very important for two finned-section missiles, where the forward fin section causes vortical interference on the tail fins. This term is negligible for missiles with a single finned section at small angles of attack.[10,11]

The objective of this research is to determine the effect of planform shape on 1) $K_{W(B)}$ and 2) planform center of pressure (CP) for supersonic missiles in cruise configurations. $K_{W(B)}$ is defined as

$$K_{W(B)} = L_{W(B)}/L_W \quad (2)$$

When $K_{W(B)}>1$, the fin-body combination increases the lift produced by the fin relative to the fin-alone case. If $K_{W(B)}<1$, the presence of the body reduces the lift produced by the fin compared to the fin-alone case.

This is the fifth paper in a series of papers from the University of Missouri-Rolla dealing with component buildup methods using the equivalent angle-of-attack method for supersonic missiles. Numerical solutions of the Euler equations have been used to explore the variation of both $K_{W(B)}$ and K_ϕ.[8,12-14] Jenn and Nelson[8] used a finite difference Euler code (SWINT) to determine K_ϕ for use in preliminary design of 2-, 3-, 4-, and 6-fin missiles for supersonic cruise at Mach numbers from 2.5 to 3.5, for positive and negative sideslip angles, and for aspect ratios from 3.2 to 4. SWINT was also used to investigate the effect of fin vertical position on $K_{W(B)}$ for delta-fin missiles.[12] The $K_{W(B)}$ data were fit to an empirical formula for easy use in preliminary design. Nelson[13] used SWINT to evaluate $K_{W(B)}$ for missiles with elliptical cross-section fuselages. He developed simple equations for $K_{W(B)}$ as a function of S/R and fuselage ellipticity for use in preliminary design. Talpallikar and Nelson[14] used a simple panel linearized potential theory (LPT) method to investigate $K_{W(B)}$ for supersonic missiles as a function of several parameters, including S/R, ϵ, τ, fuselage ellipticity and vertical position on the fuselage.

NASA has recently completed an extensive and systematic experimental program (Triservice-NASA experimental program[15,16]) to generate an aerodynamic data base to be used by missile designers. Nielsen[17] correlated some of the Triservice-NASA experimental aerodynamic data to generate useful expressions for $K_{W(B)}$ for preliminary design. These data are also valuable for diagnostic test cases for developing and evaluating computational methods.

Computational Analysis

The present research used the zonal Euler solver (ZEUS) code to solve the steady flow Euler equations using a finite-volume, predictor corrector, second-order accurate, spatial-marching approach. The predictor step advances the primitive variables using Euler's equations and the corrector step uses a modified second-order extension of Godunov's scheme which is based on the Riemann problem.[18-21] The Riemann problem represents the intersection of two two-dimensional supersonic streams. At the point of intersection, shock or expansion waves form which turn both streams to a common direction so that the pressure is the same in both streams. The resulting solutions feature constant properties along any line passing through the intersection point. The two final streams may have different densities and velocities, so a slipline usually forms between them.

The steady-state Euler equations are hyperbolic for supersonic flow. This permits marching solutions beginning from an initial data plane at the nose of the missile. To start the numerical method the bow-shock shape at the missile nose is calculated assuming a conical nose. ZEUS calculates the flowfield by marching from the initial data plane down the axis of the body; however, this marching procedure is valid only if the flow is supersonic everywhere.[18]

At a specific value of z, a grid in the crossflow plane (r-ϕ plane) is generated across the shock layer from the missile body to the bow shock. The grid is formed by dividing the crossflow plane into several zones. In the current application, zone boundaries were required to coincide with the body, the fin surfaces, and the bow shock. A coarse grid was used between the missile nose and the fin leading edge. A fine grid was used to calculate the flowfield over the fins. This approach optimized computer run time and increased the solution accuracy.

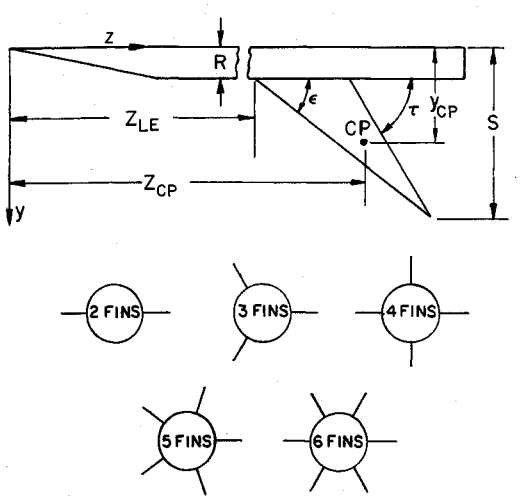

Fig. 1 Missile and fin configuration.

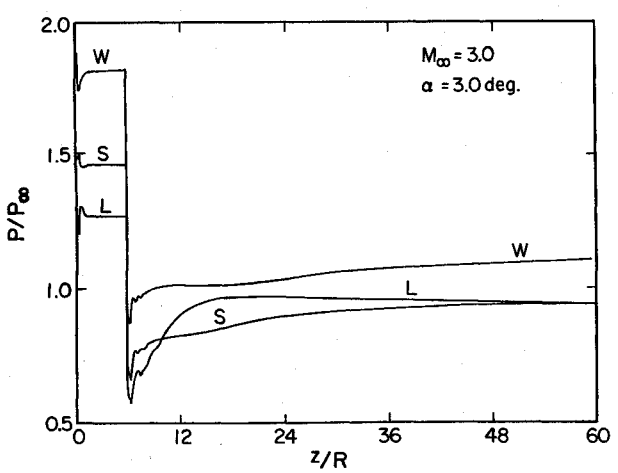

Fig. 2 Body-pressure distribution $M_\infty = 3$, $\alpha = 3$ deg.

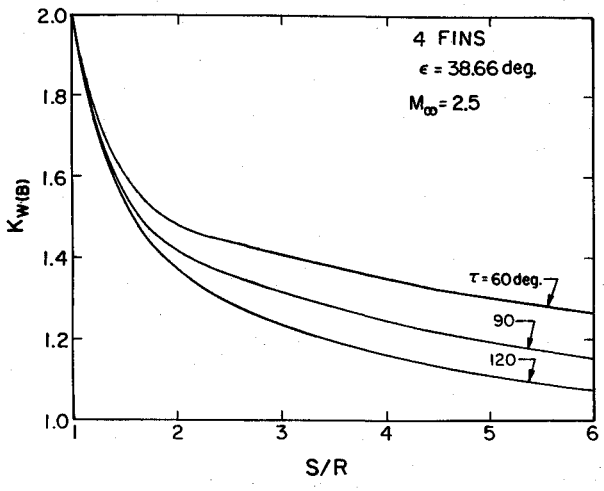

Fig. 3 $K_{W(B)}$ vs fin span, $M_\infty = 2.5$, four fins, $\alpha = 3$ deg.

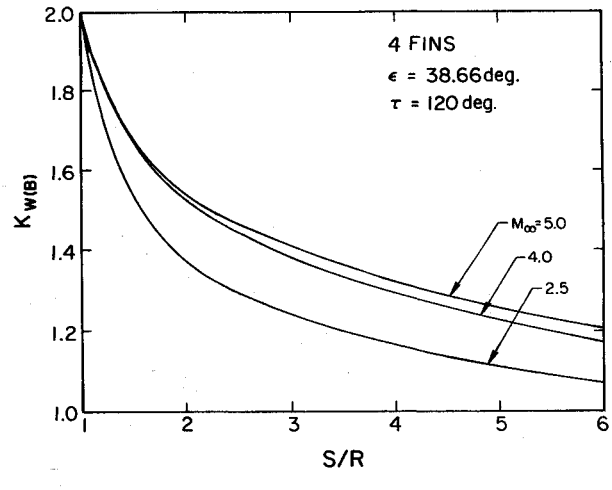

Fig. 4 $K_{W(B)}$ vs fin span, $\tau = 120$ deg, $\alpha = 3$ deg.

ZEUS calculates the fin surface-pressure distribution and integrates it over the fin surfaces to obtain fin forces $L_{W(B)}$. ZEUS fin-force predictions agree well with experimental data and other numerical results for a wide variety of missile configurations and flight conditions.[18,22-26]

The missile geometry used for this analysis had a conical nosecone with a length-to-radius ratio of 6 and a cylindrical body as shown in Fig. 1. Missiles with 2, 3, 4, 5, and 6 infinitely thin flat-plate fins spaced equally around the body circumference were analyzed. The fins were placed so that at least one fin was horizontal. $K_{W(B)}$ and CP were determined using the horizontal fin. The analysis assumes that the fins have supersonic leading edges, zero taper ratio, and, in general, swept trailing edges.

Fuselage Pressure

For this research it was important that the fin forces be independent of the shape of the nosecone and the pressure drop across the expansion fan at the nosecone-body junction; consequently, the fins were located at an axial distance far enough downstream from the missile nose so that the body pressure was constant. Figure 2 shows the leeward (L), side (S), and windward (W) surface-pressure ratios along the missile body at Mach 3. When the fins are far from the nosecone, the numerical calculations necessary to march along the body to the fin position become time consuming. Analysis of body-pressure distributions like those in Fig. 2 showed that the effects of the expansion fan from the nosecone-body junction are negligible for z/R values >22. Thus, the leading edge of the fin root chord was located at $z/R = 22$ for this research.

Wing-Alone Lift

$K_{W(B)}$ is determined by dividing $L_{W(B)}$ by the fin-alone lift, as shown in Eq. (2). ZEUS could be used to determine L_W by computing the normal force on a wing planform composed of the two fins joined together at their root chords. This procedure would be cumbersome and hard to implement. Thus, L_W was calculated from linearized supersonic theory as was done in Refs. 8, 12, and 13. For fins with supersonic leading edges, L_W is given by

$$L_W = 4\alpha q_\infty A_W / \sqrt{(M_\infty^2 - 1)} \qquad (3)$$

Missiles with large values of S/R were investigated to check the ZEUS predictions with LPT. As S/R became large, $L_{W(B)}$ predicted by ZEUS approached L_W predicted by Eq. (3). L_W from Eq. (3) was also compared with values predicted using Missile-Datcom methods.[27] The agreement was within 2% for the range of parameters considered herein. Thus, Eq. (3) was used to determine L_W for of all the cases reported herein, since fins with subsonic leading edges were not considered.

Results and Discussion

According to slender body theory (SBT), $K_{W(B)}$ is a function of fin span alone. The nonlinearity of the Euler equations suggests that $K_{W(B)}$ should be sensitive to additional parameters, such as M_∞ and α. Trailing-edge sweep and leading-edge sweep may also influence the fin forces and $K_{W(B)}$. Results presented here primarily focus on the effects of S/R, M_∞, τ and the number of fins on $K_{W(B)}$, and the fin CP location.

Missiles usually have smaller fin spans than aircraft. A survey of fin span to body radius ratio for missiles (using information from Ref. 28) showed that most missiles have S/R values between 3 and 4. In the present work S/R was varied from 1 to 6.

The ZEUS calculations were kept as simple as possible. Mesh clustering and radial zoning were not used although ZEUS has this capability. The flowfield was determined for the entire 360 deg around the missile for missiles with three and five fins, because of lack of pitch-plane symmetry. For the 2-, 4-, and 6-fin configurations, which have pitch-plane symmetry, the flowfield solution was obtained for 180 deg around the missile. A simple 18×24 grid ($\phi \times r$) with a single zone was used between the missile nose tip and $z/R = 20$. At $z/R = 20$ the ($\phi \times r$) grid was refined and zones were formed so that the fins were located at the zone edges. A 36×36 grid ($\phi \times r$) was used for the 2-, 4-, and 6-fin configurations, a 72×36 grid for the 3-fin case and a 60×36 grid for the 5-fin case. Numerical results were obtained for angles of attack from 2 to 4 deg. In this range, both $L_{W(B)}$ and L_W vary linearly with angle of attack, so the effect of changing angle of attack on $K_{W(B)}$ is negligible.

Grid sensitivity checks were made in Ref. 29 and the gridding used was a good compromise between numerical accuracy and computational run time. Numerical accuracy was hard to maintain for $S/R < 1.75$, because when the fin span was small compared to the distance between the body and the bow shock the number of grid points on the fin became small. Accuracy was improved by increasing the grid density and reducing the Courant-Fredrichs-Lewy number. Also, the curves for $K_{W(B)}$ for $1 \leq S/R \leq < 1.75$ were required to match SBT at $S/R = 1$. This assumption is acceptable because the fin-fin interference goes to zero as the fins become small[8] and SBT becomes accurate. SBT predicts that $K_{W(B)} = 2$ at $S/R = 1$, and that $K_{W(B)}$ goes to 1 as S/R becomes very large.[9]

All computations were made using the IBM 4381 computer at the University of Missouri-Rolla. CPU times of up to 2 h were required for complete flowfield solutions over the entire missile.

Flight Conditions

Cruise flight conditions were investigated in this research. The nominal case was $M_\infty = 3$, $\alpha = 3$ deg, $\epsilon = 38.66$ deg, and

$\tau = 90$ deg. This combination of ϵ and τ yields an aspect ratio of 3.2. The effect of changing the various parameters on $K_{W(B)}$ and CP was obtained by changing one parameter at a time from its nominal value.

2-, 3-, and 4-Fin Configurations

The fins are assumed to be infinitely thin, triangular flat plates; consequently, the effects of shock and expansion waves for missiles with four or fewer fins are not important. The trend in values of $K_{W(B)}$ from the ZEUS solutions are identical to the trends in $K_{W(B)}$ predicted by SBT and LPT. Figure 3 shows the variation of $K_{W(B)}$ with S/R for $\tau = 60$, 90, and 120 deg at Mach 2.5. $K_{W(B)}$ decreases as τ increases for a given value of S/R (fixed fin span). At a given S/R, the change in $K_{W(B)}$ with a change in τ is significantly greater when S/R is large.

Figure 4 shows the effect of M_∞ on $K_{W(B)}$ for $\tau = 120$ deg. $K_{W(B)}$ increases as M_∞ increases for a given value of S/R. Figures 3 and 4 show data for 4-fin missile configurations. The 2- and 3-fin results are similar, because shock and expansion waves do not affect $L_{W(B)}$ and CP for these fin configurations at small α and zero roll. Roll orientation of the fins influences the fin-fin shock and expansion wave interaction, especially at high angles of attack. These effects may be important for missiles with 3- and 4-fin configurations, but they have not been addressed herein.

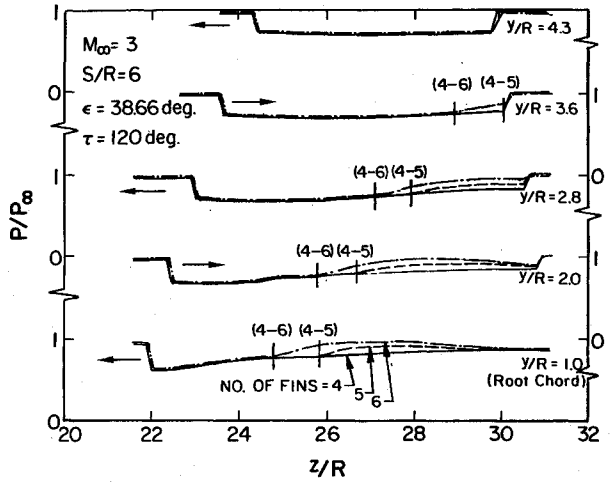

Fig. 5 Fin leeward-pressure distribution for $M_\infty = 3$, $\alpha = 3$ deg at several y/R locations; P/P_∞ scale shifted for each set of data.

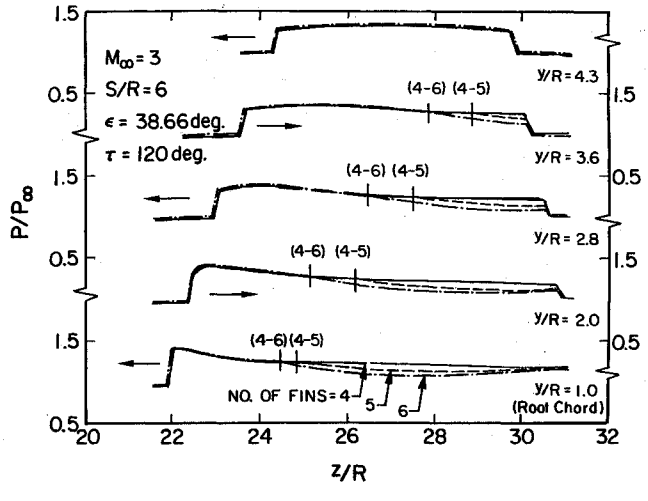

Fig. 6 Fin windward-pressure distribution for $M_\infty = 3$, $\alpha = 3$ deg at several y/R locations; P/P_∞ scale shifted for each set of data.

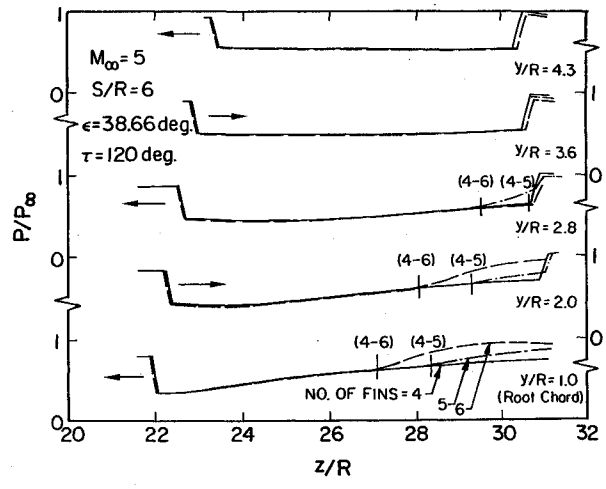

Fig. 7 Fin leeward-pressure distribution for $M_\infty = 5$, $\alpha = 3$ deg at several y/R locations; P/P_∞ scale shifted for each set of data.

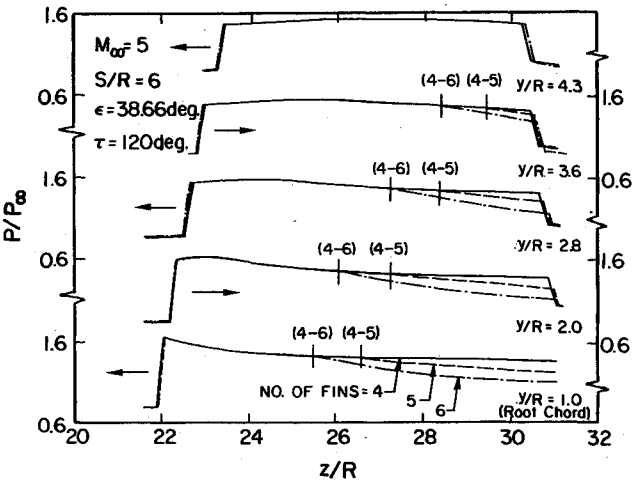

Fig. 8 Fin windward-pressure distribution for $M_\infty = 5$, $\alpha = 3$ deg at several y/R locations; P/P_∞ scale shifted for each set of data.

5- and 6-Fin Configurations

SBT predicts that $K_{W(B)}$ is independent of the number of fins because it does not allow for fin-fin interference due to shock and expansion waves. For missile configurations with five or six fins, the interaction of shock and expansion waves from the leading edge of neighboring fins becomes very important. Fin surface pressure distributions were examined to determine the position where the shock and expansion waves strike the fin planform. Their position is indicated by the distinct change in pressure on the surface of the fin. Leeward and windward fin surface-pressure for 4-, 5-, and 6-fin missiles ($M_\infty = 3$, $\alpha = 3$ deg) is shown as a function of axial location for five radial locations (y/R) in Figs. 5 and 6. The origin of the P/P_∞ scale is shifted upward by one unit for each of the five radial locations to separate the curves. The fin leading and trailing edge are indicated by the almost vertical jumps in pressure (due to shock or expansion waves from the fin of interest).

As the number of fins increases the fins become more closely placed around the fuselage and the effect of shock and expansion waves increases. The waves from the neighboring fins intersect the planform closer to the leading edge. This is illustrated in Figs. 5 and 6 for the fin leeward and windward surfaces, respectively. The axial position where the shock or the expansion waves from the neighboring fin intersect the fin planform is different for the 5- and 6-fin case. The position

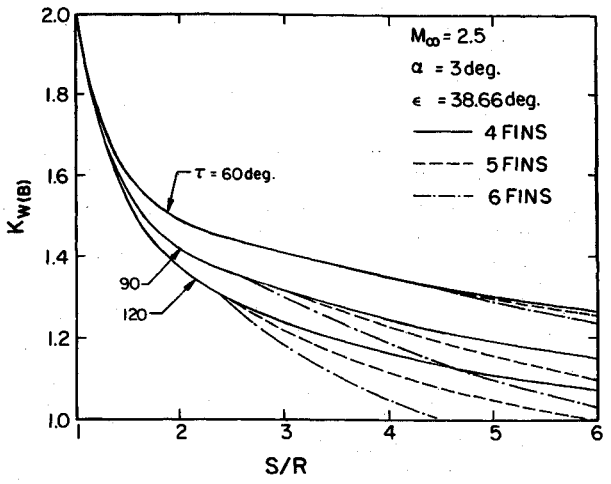

Fig. 9 $K_{W(B)}$ vs S/R, $M_\infty = 2.5$, $\alpha = 3$ deg for four, five, and six fins.

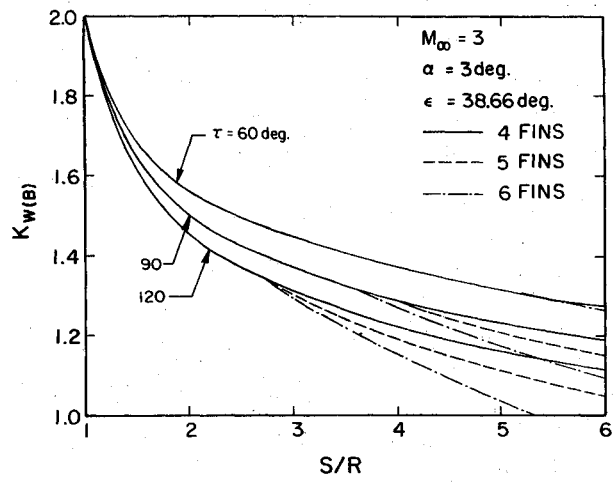

Fig. 10 $K_{W(B)}$ vs S/R, $M_\infty = 3$, $\alpha = 3$ deg for four, five, and six fins.

where the pressure for the 5-fin case breaks away from that of the 4-fin case is denoted by the vertical line labeled 4-5 and and the position where the pressure of the 6-fin case breaks away from the 4-fin case is denoted by the line labeled 4-6. The 6-fin breakaway point is always forward of the 5-fin breakaway point.

Figures 7 and 8 show fin surface-pressure distributions at Mach 5 and $\alpha = 3$ deg for $\tau = 120$ deg. Notice that the 5- and 6-fin breakaway points move aft on the fin as the Mach number increases from 3 to 5 because the neighboring fin shock and expansion wave angles decrease. Figures 5–8 clearly show the pressure jumps due to shock and expansion waves attached to the fin leading and trailing edge and demonstrate some salient features of the shock-wave and expansion-wave interactions: 1) Oblique shock and expansion waves from the leading edge of the neighboring fin usually interact with the fin planform at an axial location far behind the fin leading edge and this distance increases as M_∞ increases. 2) Shock-wave and expansion-wave interactions are restricted to an area near the trailing edge and near the wing root. Thus, they are not important for fins with small values of τ ($\tau \leq 60$ deg), because these fins have small root chords. 3) Fin-fin interactions become smaller as the Mach number increases because the breakaway point moves aft and finally behind the fin trailing edge. In other words, the fin planform area influenced by the shock and expansion waves from the neighboring fins decreases as M_∞ increases. This occurs because the shock and expansion wave angles decrease, so that the waves remain closer to the fin they emanate from.

Interference Factor $K_{W(B)}$

The pressure distributions were integrated over the fin planform to obtain $L_{W(B)}$ and, in turn, $K_{W(B)}$. Figure 9 shows the effect of shock and expansion waves on $K_{W(B)}$ for $M_\infty = 2.5$, $\alpha = 3$ deg, and $\tau = 60$, 90, and 120 deg for 4-, 5-, and 6-fin missiles. The 4-fin data are exactly the same as was shown in Fig. 3. Figures 10–12 show similar data but at $M_\infty = 3$, 4, and 5, respectively. The $K_{W(B)}$ breakaway points for the 5- and 6-fin cases are related to the pressure breakaway points shown previously in Figs. 5–8. The fin-fin shock-wave and expansion-wave interaction effects on $K_{W(B)}$ are negligible at small values of S/R (small fin spans) and for all fin configurations with small τ values (e.g., $\tau \approx 60$ deg). This is why LPT and SBT predict accurate values for $K_{W(B)}$ for $S/R \leq 2$. Table 1 presents numerical values for $K_{W(B)}$ as a function of S/R, M_∞, τ, and the number of fins. This data can be used in preliminary design for undeflected thin fins with supersonic leading edges at low angles of attack.

$K_{W(B)}$ becomes < 1 for large trailing-edge semivertex angles ($\tau \approx 120$ deg) and small Mach numbers ($M_\infty \approx 2.5$) indicating negative interference (Figs. 9 and 10). This occurs because the shock from the neighboring leeside fin increases the pressure on the leeside of the fin of interest whereas the expansion wave from the neighboring windward fin reduces the surface pressure on the windward surface of the fin of interest. These two effects combine to reduce the lift of the fin of interest and, in turn, cause $K_{W(B)}$ to become < 1.

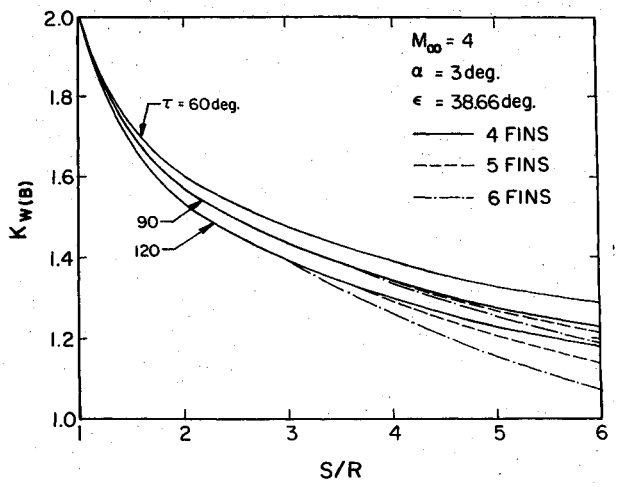

Fig. 11 $K_{W(B)}$ vs S/R, $M_\infty = 4$, $\alpha = 3$ deg for four, five, and six fins.

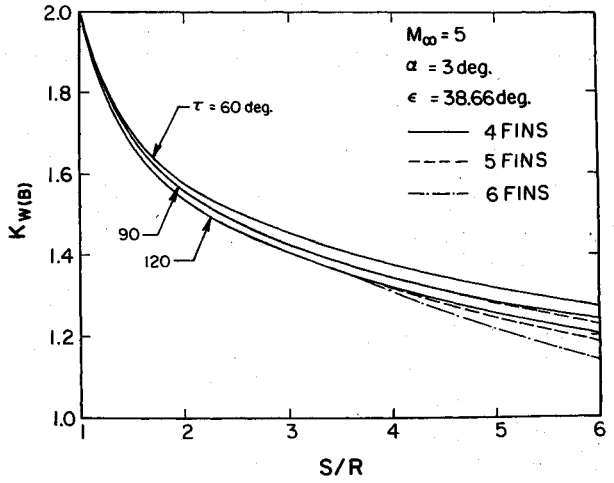

Fig. 12 $K_{W(B)}$ vs S/R, $M_\infty = 5$, $\alpha = 3$ deg for four, five, and six fins.

Table 1 Values of $K_{W(B)}$, $\epsilon = 38.66$ deg, $\alpha = 3$ deg

			S/R						
M_∞	τ, deg	Fins	2.0	3.0	4.0	4.5	5.0	5.5	6.0
2.5	60	4	1.484	1.408	1.348	1.322	1.299	1.280	1.262
2.5	60	5	1.484	1.408	1.348	1.322	1.296	1.273	1.253
2.5	60	6	1.484	1.408	1.348	1.316	1.286	1.258	1.233
2.5	90	4	1.415	1.315	1.243	1.214	1.189	1.167	1.148
2.5	90	5	1.415	1.313	1.224	1.186	1.152	1.122	1.096
2.5	90	6	1.415	1.297	1.184	1.136	1.094	1.058	1.026
2.5	120	4	1.368	1.237	1.160	1.130	1.106	1.085	1.067
2.5	120	5	1.368	1.216	1.112	1.074	1.043	1.016	0.994
2.5	120	6	1.368	1.177	1.044	0.997	0.959	0.928	0.901
3.0	60	4	1.560	1.447	1.370	1.340	1.314	1.292	1.273
3.0	60	5	1.560	1.447	1.370	1.340	1.312	1.289	1.269
3.0	60	6	1.560	1.447	1.370	1.340	1.311	1.285	1.263
3.0	90	4	1.500	1.370	1.287	1.255	1.229	1.206	1.186
3.0	90	5	1.500	1.370	1.287	1.244	1.209	1.178	1.151
3.0	90	6	1.500	1.370	1.269	1.217	1.170	1.129	1.092
3.0	120	4	1.455	1.314	1.215	1.190	1.160	1.135	1.114
3.0	120	5	1.455	1.303	1.200	1.152	1.111	1.076	1.048
3.0	120	6	1.455	1.295	1.165	1.090	1.020	0.971	0.942
4.0	60	4-5-6	1.606	1.477	1.391	1.358	1.331	1.307	1.287
4.0	90	4	1.575	1.434	1.341	1.305	1.275	1.250	1.228
4.0	90	5	1.575	1.434	1.341	1.302	1.269	1.239	1.214
4.0	90	6	1.575	1.434	1.337	1.292	1.253	1.218	1.188
4.0	120	4	1.539	1.392	1.296	1.259	1.228	1.202	1.179
4.0	120	5	1.539	1.392	1.290	1.244	1.204	1.168	1.137
4.0	120	6	1.539	1.392	1.260	1.204	1.155	1.111	1.073
5.0	60	4-5-6	1.579	1.458	1.375	1.343	1.315	1.292	1.271
5.0	90	4-5	1.559	1.428	1.342	1.309	1.281	1.257	1.236
5.0	90	6	1.559	1.428	1.342	1.309	1.281	1.249	1.222
5.0	120	4	1.538	1.408	1.317	1.282	1.251	1.225	1.202
5.0	120	5	1.538	1.408	1.315	1.279	1.240	1.209	1.181
5.0	120	6	1.538	1.408	1.307	1.256	1.211	1.172	1.137

Table 2 Center of pressure locations, $\epsilon = 38.66$ deg, $\alpha = 3$ deg

			S/R									
			2.0		3.0		4.0		5.0		6.0	
M_∞	τ, deg	Fins	z_{ND}	y_{ND}	z_{ND}	y_{ND}	z_{ND}	y_{ND}	z_{ND}	y_{ND}	z_{ND}	y_{ND}
2.5	60	4	0.640	1.350	1.277	1.684	1.907	2.020	2.540	2.360	3.175	2.705
2.5	60	5	0.640	1.350	1.277	1.684	1.907	2.020	2.537	2.356	3.172	2.705
2.5	60	6	0.640	1.350	1.277	1.684	1.907	2.020	2.451	2.368	3.175	2.735
2.5	90	4	0.821	1.356	1.630	1.704	2.441	2.062	3.245	2.420	4.056	2.790
2.5	90	5	0.821	1.356	1.630	1.704	2.422	2.065	3.215	2.448	4.006	2.840
2.5	90	6	0.821	1.356	1.627	1.708	2.407	2.092	3.170	2.500	3.956	2.910
2.5	120	4	0.996	1.363	1.970	1.722	2.933	2.089	3.889	2.460	4.861	2.840
2.5	120	5	0.996	1.363	1.955	1.726	2.873	2.116	3.794	2.516	4.760	2.905
2.5	120	6	0.996	1.363	1.922	1.742	2.790	2.161	3.713	2.572	4.696	2.965
4.0	60	4-5-6	0.627	1.325	1.239	1.628	1.850	1.933	2.467	2.244	3.084	2.560
4.0	90	4	0.817	1.330	1.622	1.644	2.426	1.963	3.230	2.292	4.037	2.620
4.0	90	5	0.817	1.330	1.622	1.644	2.426	1.963	3.225	2.292	4.019	2.630
4.0	90	6	0.817	1.330	1.622	1.644	2.426	1.966	3.215	2.304	3.994	2.665
4.0	120	4	1.005	1.335	1.995	1.660	2.977	1.993	3.954	2.332	4.934	2.680
4.0	120	5	1.005	1.335	1.992	1.660	2.966	1.996	3.911	2.352	4.852	2.720
4.0	120	6	1.005	1.335	1.992	1.662	2.933	2.011	3.830	2.392	4.733	2.790
5.0	60	4-5-6	0.625	1.321	1.236	1.621	1.845	1.921	2.454	2.222	3.066	2.528
5.0	90	4-5	0.817	1.323	1.630	1.633	2.434	1.942	3.233	2.253	4.043	2.572
5.0	90	6	0.817	1.323	1.630	1.633	2.434	1.942	3.233	2.260	4.028	2.590
5.0	120	4	1.010	1.328	2.009	1.644	2.990	1.964	3.937	2.288	4.974	2.619
5.0	120	5	1.010	1.328	2.009	1.644	2.990	1.964	3.971	2.295	4.929	2.641
5.0	120	6	1.010	1.328	2.009	1.644	2.985	1.970	3.924	2.317	4.838	2.688

Fin Center of Pressure

Figures 13–15 show the loci of center of pressure for fins with $\tau = 60$, 90, and 120 deg at $\alpha = 3$ deg for $M_\infty = 2.5$, 4, and 5, respectively. Each figure shows data for missiles with 4, 5, and 6 fins. The symbols along the curves represent a specific value of S/R. The ordinate of the figures is y_{CP}/R, where y_{CP} is the radial distance from the center of the missile to the CP measured perpendicular to the fuselage centerline. The abscissa is the distance from the missile nose to the CP position divided by the missile radius. Recall that $z_{LE} = 22R$, so $(z_{CP}/R - 22)$ is the nondimensional axial distance of the CP behind the leading edge of the fin-root chord. The effect of shock and expansion waves on the position of the center of pressure is shown by the difference between the 4-fin and the 5- or 6-fin curves. Recall that the shock and the expansion waves do not influence the 4-fin missile fin forces and moments at small α. Generally, CP moves radially outward and axially forward due to shock and expansion waves from the neighboring fins as the number of fins increases from four to six at a specific M_∞.

The effect of changing M_∞ on the CP is obtained by comparing Figs. 13–15. Generally, CP moves radially inward and axially rearward as the M_∞ increases for 5- and 6-fin missiles.

In general, for a fixed fin size (S/R) the center of pressure moves axially forward and radially outward as the number of fins increases. Increasing τ while holding M_∞ and S/R constant tends to move the CP aft and slightly outward. These rather small movements in the fin CP location may be very

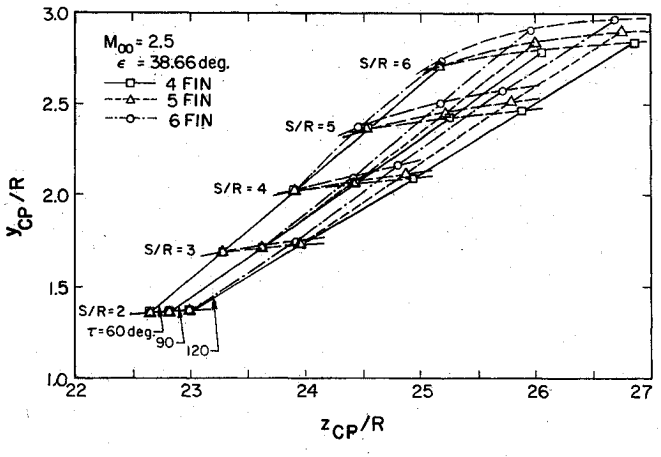

Fig. 13 Fin CP location for $M_\infty = 2.5$, $\alpha = 3$ deg, $\tau = 60$, 90, and 120 deg for 4-, 5-, and 6-fin missiles.

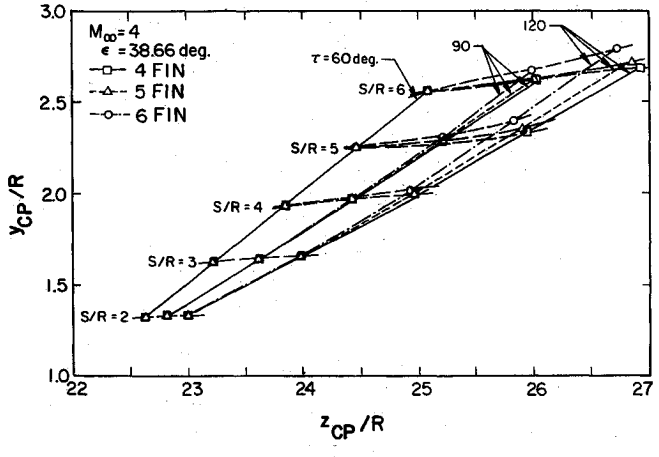

Fig. 14 Fin CP location for $M_\infty = 4$, $\alpha = 3$ deg, $\tau = 60$, 90, and 120 deg for 4-, 5-, and 6-fin missiles.

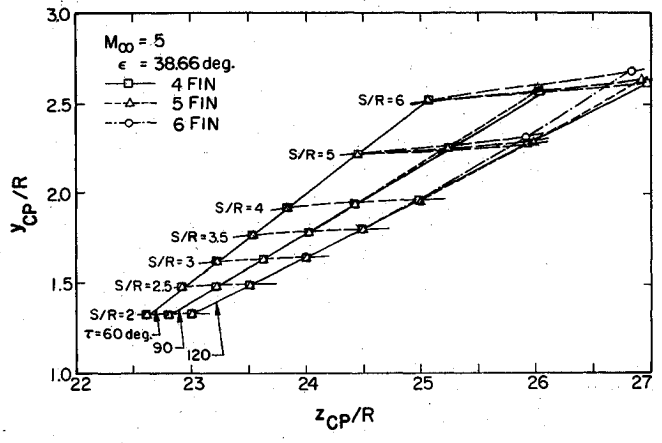

Fig. 15 Fin CP location for $M_\infty = 5$, $\alpha = 3$ deg, $\tau = 60$, 90, and 120 deg for 4-, 5-, and 6-fin missiles.

important for stability and control. As M_∞ increases from 2.5 to 5, the CP location moves as much as 2% forward for the 6-fin case for $\tau = 90$ deg and moves up to 4% forward for $\tau = 120$ deg. Fin CP locations for Mach 2.5, 4, and 5 for $\tau = 60$, 90, and 120 deg are tabulated in Table 2 for use in preliminary design for undeflected thin fins with supersonic leading edges at low angles of attack.

Conclusions

Values of $K_{W(B)}$ and CP for supersonic missiles with 2-, 3-, 4-, 5-, and 6-fin configurations have been determined for values of S/R ranging from 1 to 6 as a function of M_∞ and τ using an Euler solver, ZEUS. $K_{W(B)}$ and CP are sensitive to S/R and τ in agreement with SBT. However, SBT and LPT ignore the fin-fin interference effects due to shock and expansion waves, so $K_{W(B)}$ and CP results for 5- and 6-fin configurations are significantly different from SBT and LPT predictions. The fin $K_{W(B)}$ value and CP location must be accurately known for fin hinge-moment predictions.

Fin pressure distributions are analyzed to study fin-fin interference due to shock and expansion waves. The values of S/R where 5- and 6-fin values of $K_{W(B)}$ break away from the 4-fin value are directly related to the position at which the shock and expansion waves originating from adjacent fins strike the fin planform. Shock and expansion waves have a negligible effect on $K_{W(B)}$ and CP for small fins ($S/R < 3.5$) and for fins with τ less than about 80 deg. For 6-fin missiles with large S/R and large τ the shock and expansion waves from the adjacent fins cause $K_{W(B)}$ to become < 1. This implies that the fin-fin interference actually decreases the lift or, in other words, produces destructive interference.

The expansion and shock waves from the adjacent fins also affect the fin CP location. Increasing S/R moves CP rearward and outward on the fin planform. For 5- and 6-fin missiles at a specific S/R, CP usually moves inward and aft as M_∞ increases. This influences both the pitching and rolling moments of the missile. Also, locating the fin forward on the missile body, close to the nosecone-body junction point, can dramatically influence the value of $K_{W(B)}$ and CP due to the effect of expansion waves from the nosecone-body junction.

Tables are presented for $K_{W(B)}$ and CP as a function of S/R, M_∞, τ, and number of fins. They provide sufficient information to incorporate $K_{W(B)}$ and fin CP position into a preliminary or conceptual design tool which, when coupled with the equivalent angle-of-attack method, will give improved predictions for missile fin forces.

Future $K_{W(B)}$ and CP calculations should be extended to nonconventional missile body cross-section shapes such as squares or triangles and to high angles of attack. Also, the magnitude of the hinge moments and the effects of flap deflection on the movement of the CP need to be evaluated.

Acknowledgments

This work was supported by McDonnell Douglas Missile Systems Company, St. Louis, Missouri, through the Independent Research and Development Program, monitored by John E. Williams and Kurt D. Bausch. Additional funds were provided by the Missouri Research Assistance Act.

References

[1]Sun, J., and Cummings, R. M., "Evaluation of Missile Aerodynamic Characteristics Using Rapid Prediction Techniques," *Journal of Spacecraft and Rockets,* Vol. 21, No. 6, 1984, pp. 513–520.

[2]Pitts, W. C., Nielsen, J. N., and Kaattari, G. E., "Lift and Center of Pressure of Wing-Body-Tail Combinations at Subsonic, Transonic, and Supersonic Speeds," NACA Rept. 1307, 1957.

[3]Hemsch, M. J., and Nielsen, J. N., "Equivalent Angle-of-Attack for Estimating Nonlinear Aerodynamics of Missile Fins," *Journal of Spacecraft and Rockets,* Vol. 20, No. 4, 1981, pp. 356–362.

[4]Hemsch, M. J., and Nielsen, J. N., "Extension of Equivalent Angle-of-Attack Method for Nonlinear Flows," *Journal of Spacecraft and Rockets,* Vol. 22, No. 3, 1983, pp. 304–308.

[5]Stoy, S. L., and Vukelich, S. R., "Extension of Equivalent Angle-of-Attack Prediction Method," AIAA Paper 84-0311, Jan. 1984.

[6]Stoy, S. L., and Vukelich, S. R., "Prediction of Aerodynamic Characteristics of Unconventional Missile Configurations Using Component Build-Up Techniques," AIAA Paper 86-0489, Jan. 1986.

[7]Nielsen, J. N., "Nonlinearities in Missile Aerodynamics," AIAA Paper 78-20, Jan. 1978.

[8]Jenn, A. A., and Nelson, H. F., "Sideslip Effects on Fin-Fin Interference in Supersonic Missile Aerodynamics," *Journal of Spacecraft and Rockets,* Vol. 25, No. 6, 1988, pp. 385–392.

[9]Nielsen, J. N., *Missile Aerodynamics,* McGraw-Hill, New York, 1960, pp. 113–143.

[10]Nielsen, J. N., "Missile Aerodynamics—Past, Present and Future," *Journal of Spacecraft and Rockets,* Vol. 17, No. 3, 1980, pp. 165–176.

[11]Hemsch, M. J., and Nielsen, J. N., "The Equivalent Angle-of-Attack Concept for Engineering Analysis," *Tactical Missile Aerodynamics,* edited by M. J. Hemsch and J. N. Nielsen, Progress in Astronautics and Aeronautics, Vol. 104, AIAA, New York, 1986, pp. 482–518.

[12]Jenn, A. A., and Nelson, H. F., "Wing Vertical Position Effects on Lift for Supersonic Delta Wing Missiles," *Journal of Spacecraft and Rockets,* Vol. 26, No. 4, 1989, pp. 210–216.

[13]Nelson, H. F., "Wing-Body Interference Lift for Supersonic Missiles with Elliptical Cross-Section Fuselages," *Journal of Spacecraft and Rockets,* Vol. 26, No. 5, 1989, pp. 322–329.

[14]Talpallikar, M. V., and Nelson, H. F., "Modeling Supersonic Missile Fin-Body Interference for Preliminary Design," *Journal of Spacecraft and Rockets,* Vol. 27, No. 6, 1990, pp. 571–576.

[15]Hemsch, M. J., and Nielsen, J. N., "Triservice Program for Extending Missile Aerodynamic Data Base and Prediction Programs Using Rational Modeling," Nielsen Engineering and Research, TR 249, Mountain View, CA, 1981.

[16]Allen, J. M., Shaw, D. S., and Sawyer, W. C., "Analysis of Selected Data From the Triservice Missile Data Base," AIAA Paper 89-0478, Jan. 1989.

[17]Nielsen, J. N., "Supersonic Wing-body Interference at High Angles of Attack with Emphasis on Low Aspect Ratios," AIAA Paper 86-0568, Jan. 1986.

[18]Wardlaw, A. B., Jr., and Davis, S. F., "A Second Order Godunov Method for Tactical Missile," Naval Surface Weapons Center, NSWC TR 86-506, Silver Spring, MD, Dec. 1986

[19]Holt, M., *Numerical Methods in Fluid Dynamics,* Springer Series in Computational Physics, Springer-Verlag, Berlin, 1977, pp. 41–56.

[20]Davis, S. F., "Simplified Second-Order Godunov-Type Methods," *SIAM Journal on Scientific and Statistical Computing,* Vol. 9, No. 3, 1988, pp. 445–473.

[21]Glaz, H. M., and Wardlaw, A. B., Jr., "A High-Order Godunov Scheme for Steady Supersonic Gas Dynamics," *Journal of Computational Physics,* Vol. 58, No. 2, 1985, pp. 157–187.

[22]Wardlaw, A. B., Jr., Priolo, F. J., Solomon, J. M., and Baltakis, F. P., "Inviscid Multiple Zone Calculations for Supersonic Tactical Missiles," AIAA Paper 84-2099, Aug. 1984.

[23]Priolo, F. J., and Wardlaw A. B., Jr., "A Comparison of Inviscid Computational Methods for Supersonic Tactical Missiles," AIAA Paper 87-0113, Jan. 1987.

[24]Wardlaw, A. B., Jr., Baltakis, F. P., Martin, F. M., Priolo, F. J., and Jettmar, R. U., "Godunov's Method for Supersonic Tactical Missile Computations," *Journal of Spacecraft and Rockets,* Vol. 24, No. 1, 1987, pp. 40–47.

[25]Evans, J., and Wardlaw, A. B., Jr., "Prediction of Tubular Projectile Aerodynamics Using the ZEUS Code," AIAA Paper 89-0334, Jan. 1989.

[26]Priolo, F. J., and Wardlaw, A. B., Jr., "Induced Roll Computations for Conventional Missiles," AIAA Paper 89-0331, Jan. 1989.

[27]Vukelich, S. R., "Development Feasibility of Missile Datcom," Air Force Wright Aeronautical Lab., AFWAL-TR-81-3130, Wright-Patterson AFB, OH, Oct. 1981.

[28]*Jane's Weapon Systems 1987-88,* 18th ed., edited by B. Blake, Jane Publishing Co. Ltd., London, 1987, pp. 1016–1028.

[29]Talpallikar, M. V., "Numerical Solutions to Wing-Body Interference of Missiles in Supersonic Flow, Master's Thesis, Univ. of Missouri-Rolla, Rolla, MO, May 1989.